European Congress on Computational Methods in Applied Sciences and Engineering
ECCOMAS 2000
Barcelona, 11-14 September 2000

PREDICTION OF QUASI-STATIONARY AERODYNAMIC COEFFICIENTS USING THE ALE METHOD

J. Cormier*, S. Champagneux*, V. Moreux†, and R. Collercandy†

*European Centre for Research and Advanced Training in Scientific Computation (CERFACS), 42, Avenue Gaspard Coriolis. 31057 Toulouse Cedex 01, France. web page: http://www.cerfacs.fr/

†Aerospatiale Matra Airbus, BP M0142/3, 316 route de Bayonne, 31060 Toulouse Cedex 3, France. web page: http://www.aeromatra.com

Key words: Dynamic Derivatives, Flight Stability, ALE, Moving Grid, Navier-Stokes, CFD

Abstract. *A method for the computation of steady dynamic derivatives of aircraft is described. Viscous simulations are performed with a multiblock, structured code, using an ALE (Arbitrary Lagrangian Euler) finite volume formulation. The method was first tested on a simple tri-dimensional wing and horizontal tailplane. The results were compared with an engineering method, for which good accuracy is expected on these test cases. Calculations were then performed on a complex Airbus civil aircraft configuration. On this geometry, the results show good agreement with wind tunnel test measurements.*

1 INTRODUCTION

Stability derivatives of an aircraft are the derivatives of all aerodynamic forces and moments with respect to the independent variables of flight. They allow the characterization of aircraft behavior in any flight conditions. These coefficients are essential for aircraft manufacturers for the aircraft stability study, and for the fine tuning of control laws.

Most coefficients related to the flow velocity may be obtained by wind tunnel experiments with sufficient accuracy. The estimation of dynamic derivatives using wind tunnel tests is less accurate : the most frequently used technique (the forced oscillation technique) implies parasitic forces, especially inertia forces and model distortion, which are dominant with respect to aerodynamic forces. Therefore, the availability of a reliable and accurate numerical prediction method for dynamic derivatives would be a great help for the aircraft manufacturer. Furthermore, the cost reduction related to the reduction of wind tunnel tests would be significant.

The objective of the present study is to show the ability of a Navier-Stokes solver, NSMB[1], to properly calculate the damping derivatives for typical civil aircraft configurations, performing any kind of motion using ALE method (Arbitrary Lagrangian Eulerian). The study is limited to the steady case, i.e. to derivatives related to angular velocities.

In this paper, the numerical aspects are first presented. A simple test case, based on the ONERA M6 wing geometry is then investigated for validation purpose. Finally, an application is performed on a complex geometry, a transport civil aircraft, consisting of a fuselage, a wing and the horizontal and vertical tailplanes.

2 GOVERNING EQUATIONS

We solve the tri-dimensional unsteady compressible Navier-Stokes equations, which conservative form in a moving frame can be expressed as :

$$\frac{\partial}{\partial t}\iint_{\Omega(t)} \vec{Q}(x,\tau)\, d\Omega + \int_{\partial\Omega(t)} \vec{\vec{H}}.\vec{n}\, dS = \vec{0} \ , \tag{1}$$

where the control volume $\Omega(t)$ and its boundary $\partial\Omega(t)$ are time-dependent, and with :

$$\vec{Q} = \begin{pmatrix} \rho \\ \rho\vec{V} \\ \rho E \end{pmatrix} \ , \quad \vec{\vec{H}}.\vec{n} = \left[(\vec{V} - \vec{\dot{x}}).\vec{n}\right]\vec{Q} + \begin{pmatrix} 0 \\ P\ \vec{n} \\ P\vec{V}.\vec{n} \end{pmatrix} - \begin{pmatrix} 0 \\ \vec{\vec{\Sigma}}.\vec{n} \\ (\vec{\vec{\Sigma}}.\vec{V}).\vec{n} + k\vec{\nabla}T.\vec{n} \end{pmatrix} \ ,$$

where ρ, $\vec{V}$, E, P and $\vec{\vec{\Sigma}}$ are respectively the density, the velocity vector, the total energy, the pressure and the shear stress tensor. The flux $\vec{\vec{H}}.\vec{n}$ is decomposed into three components, the convective flux, the pressure contribution and the viscous flux. $\vec{n}$ denotes the outward normal of the moving boundary $\partial\Omega(t)$ which has a velocity $\vec{x}$.

To close the system, the gas is assumed to be thermally and calorically perfect providing the state equation :

$$E = \frac{P}{(\gamma - 1)\rho} + \frac{|\vec{V}|^2}{2} \quad , \tag{2}$$

For the viscous fluxes, Sutherland's law is used to determine the molecular viscosity μ, and the heat conductivity constant k is found assuming a constant Prandtl number (0.72 in all cases).

3 FLOW SOLVER

The NSMB solver is developed in the frame of the European Academia-Industry consortium[1] : Aerospatiale Matra (France), SAAB (Sweden), CERFACS (France), EPFL (Switzerland) and KTH (Sweden). The NSMB code is a parallelized Multi-Block Navier-Stokes solver based on a finite volume approach. It uses a dynamic allocation and database manager.

This solver is used in the aircraft design process of Aerospatiale Matra Airbus. To achieve that goal, runs can be made on various computers and the numerical code is optimized for use on vector computers as well as on scalar machines. It has been written in parallel with a Message Passing Paradigm (MPI) to deal with this kind of complex geometries which demand powerful resources.

4 NUMERICAL METHODS AND TURBULENCE MODELS

The Navier-Stokes equations are discretized using a space centered finite volume[2] with second order artificial dissipation terms. The equations are integrated in time using the implicit LU-SGS (Lower-Upper Symmetric Gauss-Seidel) scheme[3].

Turbulence in boundary layer is modeled using either the algebraic model of Baldwin-Lomax[4] or the one-equation model of Spalart-Allmaras[5]. At last, characteristic boundary conditions were used to model the far-field, and the solid wall is modeled using a adiabatic non-slip condition.

5 CALCULATION OF DYNAMIC DERIVATIVES

5.1 Notations

Figure 1 presents the different notations, used in this paper, and in particular, the force components C_x, C_y and C_z, and the moment components C_l, C_m and C_n. The wingspan is called b, the mean aerodynamic chord C_0 and the aerodynamic center F. At last, p, q and r and the angular velocities.

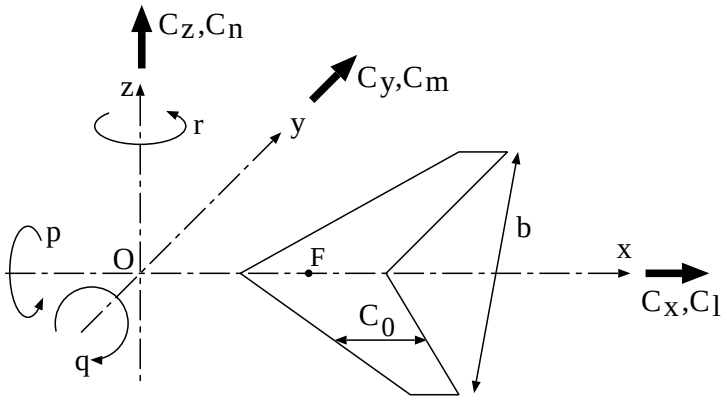

Figure 1: Notations

5.2 Introduction to dynamic derivatives

The stability derivatives represent the coefficients of a Taylor series expansion of the aerodynamic forces and moments of a configuration, which is subjected to a small perturbation of the independent flight variables (velocity magnitude (V), angle of attack and sideslip (α, β), angular velocity (p, q, r), acceleration ($\dot{\alpha}$, $\dot{\beta}$), etc...). For instance, in the longitudinal case we can write :

$$C_x(\alpha, q, \dot{\alpha}) \approx C_{x_0} + \alpha \,.\, C_{x_\alpha} + q \,.\, C_{x_q} + \dot{\alpha} \,.\, C_{x_{\dot{\alpha}}} \quad , \tag{3}$$

where : $C_{x_\alpha} = \frac{\partial C_x}{\partial \alpha}\Big)_0$, $C_{x_q} = \frac{\partial C_x}{\partial q}\Big)_0$ and $C_{x_{\dot{\alpha}}} = \frac{\partial C_x}{\partial \dot{\alpha}}\Big)_0$ are the longitudinal derivatives, estimated at equilibrium position ($\alpha = q = \dot{\alpha} = 0$).

We can distinguish static derivatives, steady dynamic derivatives and unsteady dynamic derivatives. Static derivatives are terms due to variations of the linear velocities. Steady dynamic derivatives are terms related to angular velocity. Unsteady dynamic derivatives are terms due to variations of linear accelerations.

In this study, we focus on static derivatives and steady dynamic derivatives (also called quasi-stationary aerodynamic coefficients). Assuming that efforts vary linearly, we can approach the derivatives by the rate of growth between two different states. For instance, the lift derivative related to a pitching motion will be approximated by :

$$C_{z_q} = \frac{C_z(q) - C_z(q=0)}{q} \quad . \tag{4}$$

In the case of static derivatives, the two calculations are static calculations, but in the case of steady dynamic derivatives, we have to simulate at least one calculation of rotating flow (p, q, $r \neq 0$).

5.3 Arbitrary Lagrangian-Eulerian formulation

In order to account for the rotation of the computational domain, an Arbitrary Lagrangian-Euler (ALE) method has been used. This method, initially developed by Donea et al.[6] for unsteady fluid-structure computations, consists in performing the Finite-Volume integration of the Navier-Stokes equations over a moving and deforming cell (eqn. 1).

It leads to modifying the convective fluxes, including a grid velocity, but does not add any source terms to the conservation equation, in contrast to the rotating frame formulation of the Navier-Stokes equations[7]. Thus, the convergence properties of the implicit method are preserved, without having to treat a source term implicitly.

The implementation of this method is quite elementary. The Jameson numerical flux $\vec{\vec{H}}_{Jameson}.\vec{n}$ is modified as shown in eqn. 5.

$$\vec{\vec{H}}_{Jameson_{ALE}} = \vec{\vec{H}}_{Jameson} - (\vec{\dot{x}}.\vec{n})\,\vec{\vec{I}} \tag{5}$$

Concerning the calculation of the artificial dissipation, we have to subtract $\vec{\dot{x}}.\vec{n}$ from the eigenvalues of the flux Jacobian matrix. Boundary conditions are modified to take into account the grid velocity, and a local pressure gradient due to the movement of the solid wall has to be added in the solid wall boundary condition[7].

The general formulation of ALE allows to solve fluid dynamic problems with the Eulerian approach ($\vec{\dot{x}} = \vec{0}$), the Lagrangian approach ($\vec{\dot{x}} = \vec{V}$), or any other approaches with moving and deforming frames.

The ALE method used in this study is slightly simplified with regard to Donea's formulation. The grid velocity is given by $\vec{\Omega} \wedge \overrightarrow{OM}$, where $\vec{\Omega}$ is the constant angular velocity. The mesh is moving, but not deforming, so no geometric conservation law is used. Furthermore, the mesh coordinates do not have to be updated at each time-step, since the

mesh performs a block-rotation in this particular case, and so computing time is saved. At last, because the studied rotations are very small, the pressure gradient at the wall surface has been neglected.

6 ONERA M6 WING

We first validate our implementation on the well-known ONERA M6 wing. This is a swept back wing, designed to be used as an experimental support for CFD validation at high Reynolds numbers[8]. The Reynolds number, based on the mean aerodynamic chord is 11.74 million, and the Mach number varies from 0.5 to 0.7. We chose small angles of attack ($< 3.08°$) so that the flow remains subsonic.

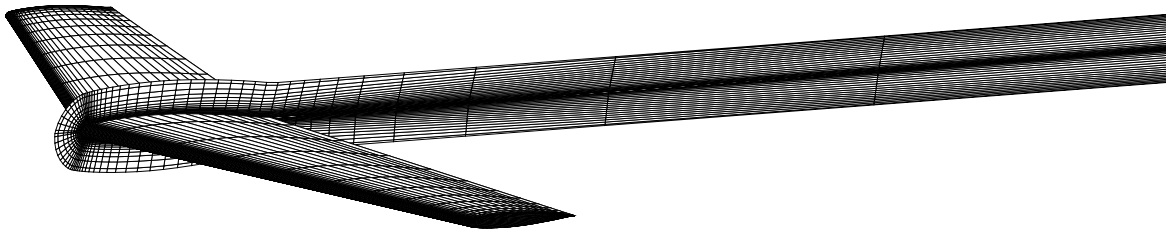

Figure 2: Mesh used for Navier Stokes simulations

Two meshes were used. The first one is designed for Euler simulations and contains 38 blocks and 148758 nodes. The second, derived from the first one, is used for Navier-Stokes simulations (Fig. 2). It contains 60 blocks and 237836 nodes and the size of near wall cells is about $y^+ = 1$. The outer boundaries are located 12 chord lengths away from the airfoil.

We present successively preliminary tests, validation in lateral cases, and validation in longitudinal cases. In order to improve understanding, we shortly describe the physical phenomena for each motion [9], [10].

6.1 Static longitudinal case

We first performed static simulations to ensure that the modeling (grid, schemes, models, ...) was accurate. We used successively Euler formulation, Baldwin-Lomax model and Spalart-Allmaras model to estimate the influence of turbulence modeling on the solution.

As shown in Tab. 1, the position of the aerodynamic centre and the lift-curve slope C_{z_α} are well predicted, even with an Euler simulation. On the contrary, because viscous drag is not negligible, Euler calculations do not allow the prediction of the drag coefficient.

	Measurements	NSMB Euler	NSMB BL	NSMB SpA
x_F	25 $\%C_0$	24.9 $\%C_0$	24.7 $\%C_0$	24.8 $\%C_0$
$C_{z_\alpha}(M = 0.5)$	4.00	4.00	4.02	-
$C_{z_\alpha}(M = 0.7)$	4.33	4.50	4.41	4.36

Table 1: Static results at angle of attack of 0 degrees

We performed a viscous simulation at Mach number 0.7 and angle of attack 1.08 degrees, to compare the local pressure load with experimental data on 7 different sections along the span. In figure 3 we present results in two sections ($y = 20\%b$ and $y = 99\%b$). As we can see, numerical results are in very good agreement with experimental data, even near the wing tip. Comparison over all other sections are also very good.

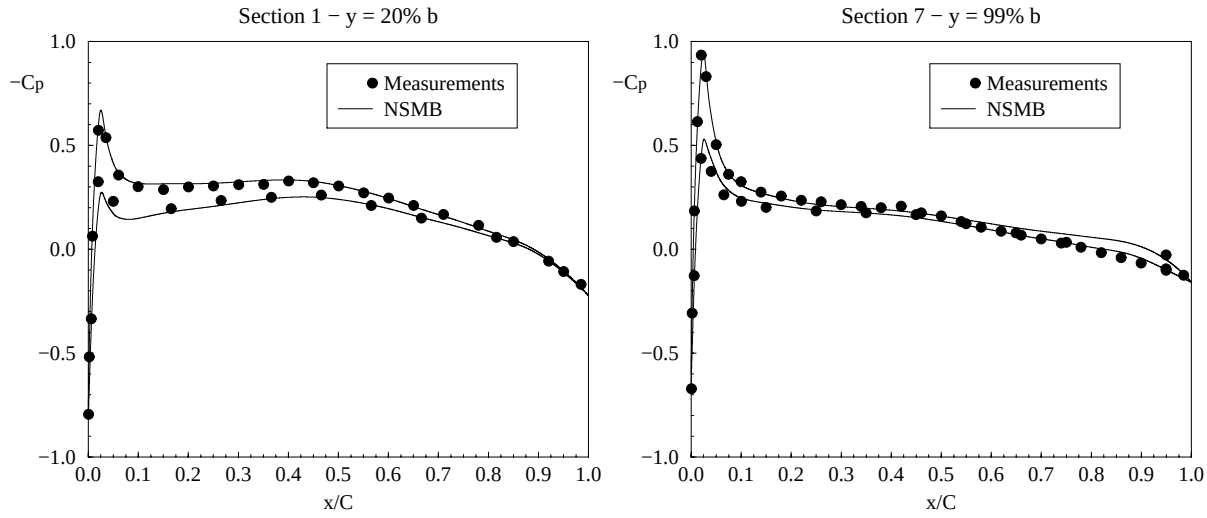

Figure 3: Pressure coefficient on two sections

These results confirm that the problem is well modeled. Moreover, we saw that Euler simulations are sufficient to predict phenomena governed by the lift like C_z, C_l, C_m and their derivatives. For the other coefficients : C_x, C_y and C_n, viscous calculation are necessary. Because we focus on all the phenomena, we only present viscous calculations.

6.2 Lateral cases

In this part, sideslip, yawing and rolling effects are studied. The results are compared with data provided by the engineering method ESDU (cf [11]). All simulations were performed at an angle of attack of 2 degrees. We used the Baldwin-Lomax model, which is accurate on such lifting configuration (cf § 6.1).

Sideslip effect In case of sideslip, even in absence of dihedral, a flat lifting wing has a C_{l_β}, due to its swept back geometry. According to simple swept back theory, the velocity normal to the wing reference line (1/4 chord line for subsonic, leading edge for supersonic) determines the lift.

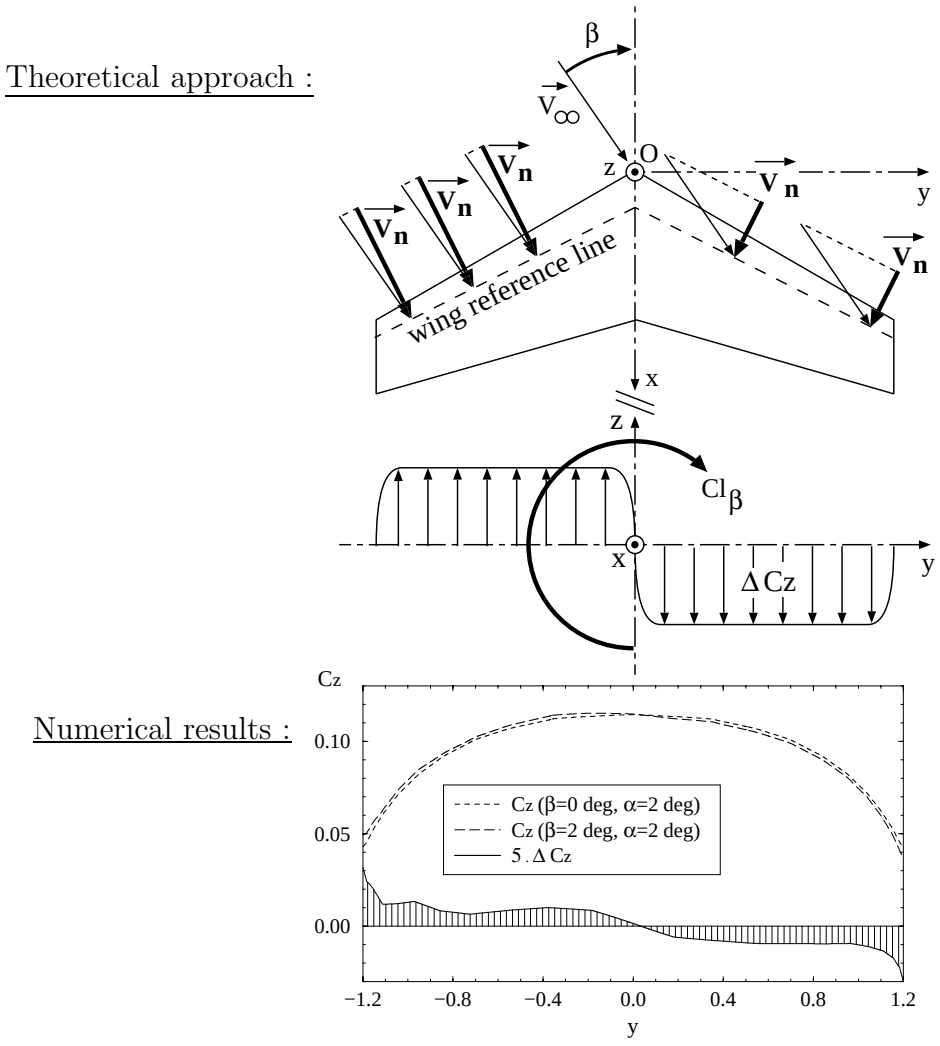

Figure 4: Sideslip description and numerical results

Sideslip angle unbalances this normal velocity field between the two sides of the wing (Fig. 4 - Theoretical approach). It follows obviously that it creates a positive and constant incremental lift on the right wing and a negative and constant incremental lift on the left wing. This lift unbalance generates a negative rolling moment C_{l_β}. The non-zero C_{n_β} and C_{y_β} are secondary effects, mainly due to the modification of the induced drag distribution along the span. They are negative and positive respectively.

	ESDU	NSMB
C_{y_β}	0	0.010
C_{l_β}	-0.11	-0.117
C_{n_β}	0	-0.026

Table 2: Sideslip effect result

To increase the visibility, we multiplied the incremental lift by 5 (Fig. 4 - Numerical results). As we can see its distribution is in fair agreement with the theoretical prediction : the incremental lift is nearly constant on each side of the wing. Moreover, as shown in Tab. 2, C_{l_β} is well predicted by the code. At last, whereas in absence of dihedral angle, the ESDU method is insufficient to predict lateral effects, the code predicts non-zero values for C_{n_β} and C_{y_β} and the sign is respected.

Rolling effect When a wing rolls with angular velocity p about its longitudinal axis, it affects instantaneously the local angle of attack at all stations of the wing. This angle of attack varies linearly across the span, from $-\frac{p^* b}{2}$ to $\frac{p^* b}{2}$ (Fig. 5 - Theoretical approach). This antisymmetric α distribution produces an antisymmetric and linear increment in the lift distribution, and so a negative rolling moment, the damping-in-roll derivative C_{l_p}. As for sideslip effect, C_{n_p} and C_{y_p} are effects governed by the distribution of induced drag, but with higher intensity.

As we can see, the lift distribution is in good agreement with the theoretical prediction (Fig. 5 - Numerical results) : the incremental lift induced by the rolling motion varies linearly along the span. Furthermore, the rolling effect predicted by the code is in fair agreement with the ESDU data (Tab. 3).

	ESDU	NSMB
C_{y_p}	0.15	0.120
C_{l_p}	-2.16	-2.43
C_{n_p}	-0.23	-0.226

Table 3: Rolling effect result

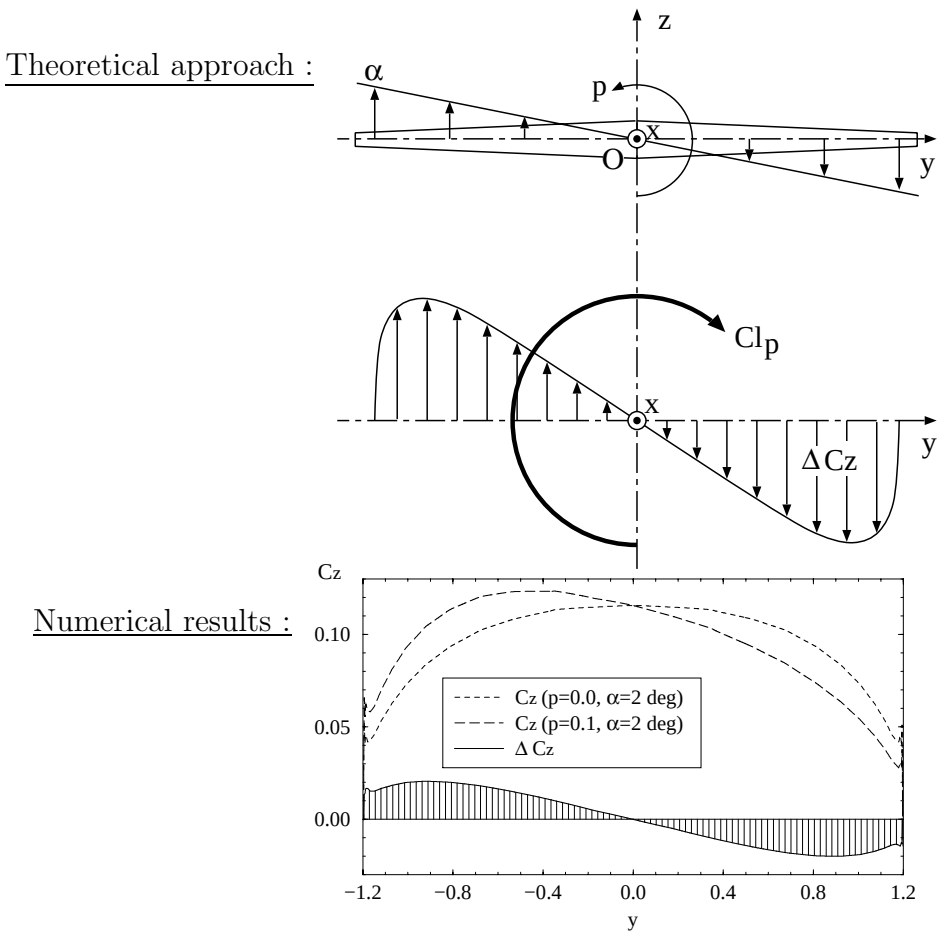

Figure 5: Rolling description and results

Yawing effect When a wing has a rate of yaw r superimposed on the forward motion, its velocity field is altered significantly. Because of the swept back geometry of the wing and the yawing motion, the normal velocity field varies almost linearly along the span (Fig 6 - Theoretical approach). This phenomenon unbalances the drag distribution along the span (even in absence of lift because of viscous effects), and creates a negative yawing moment, the damping-in-yaw derivative C_{n_r}, which resists to yawing motion. This unbalance also creates a lateral force C_{y_r}. Simultaneously, because the profile is lifting, the antisymmetric change of the velocity field induces an antisymmetric increment in the lift distribution, and so a rolling moment C_{l_r}.

In this case, C_{l_r} is only due to lift and so the numerical result is in good agreement with the ESDU data (Tab. 4). The value obtained for C_{n_r} is not so good. Many reasons can explain this error. First of all, this coefficient is so small that the absolute error due to

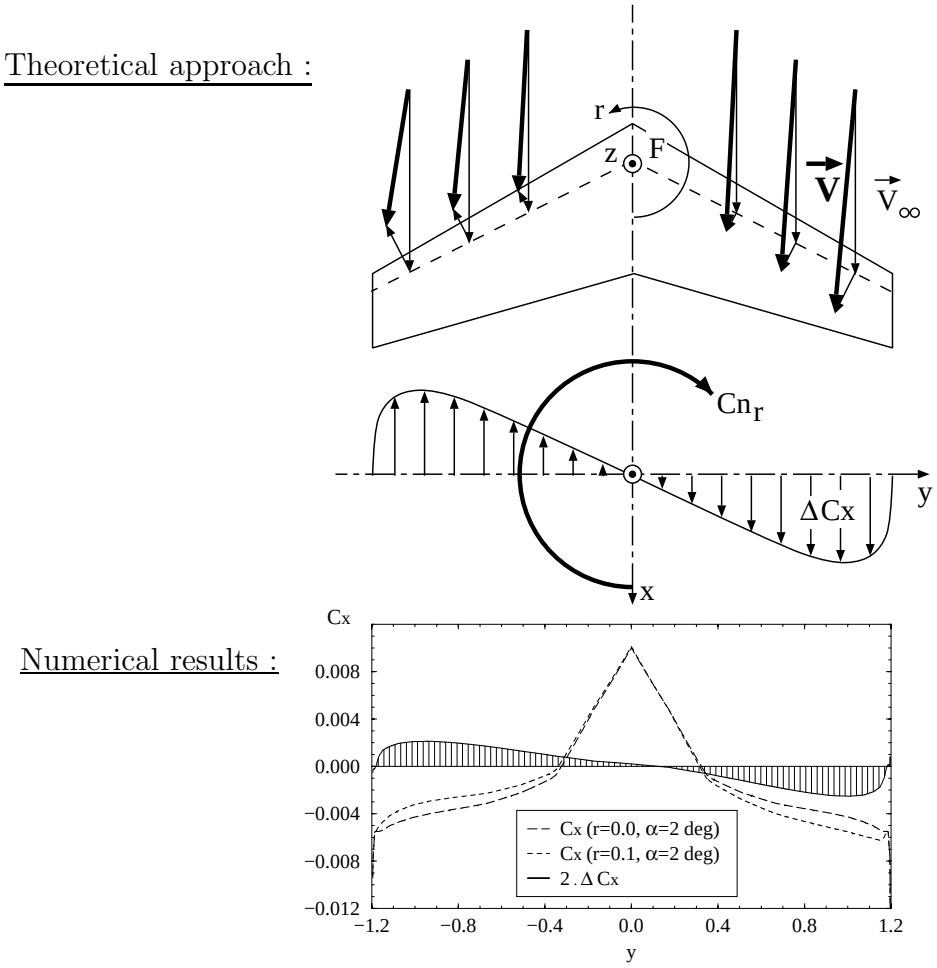

Figure 6: Yawing description and results

approximations in the ESDU formulation and due to the discretization in the numerical methods, becomes very important. Furthermore, this coefficient is mainly due to drag phenomena, which are much more difficult to estimate than lift. Nevertheless, the sign of this coefficient is correct, and the drag distribution is in good agreement with the theoretical approach (Fig. 6 - Numerical results).

Conclusion In this part we have shown that ALE method is able to predict stability derivative coefficients with a good level of accuracy. In the case when phenomena are governed by lift, results are in good agreement with the ESDU data. In the other case, results are satisfying in comparison with currently available models.

	ESDU	NSMB
C_{y_r}	-	0.010
C_{l_r}	0.30	0.261
C_{n_r}	-0.02	-0.011

Table 4: Yawing effect result

6.3 Dynamic longitudinal case

In this part we focus on phenomena due to the pitching of an horizontal stabilizer. The main objective is to validate a relationship between the pitch damping coefficient C_{z_q} and the lift-curve slope C_{z_α}.

6.3.1 Geometric approach

When the wing represents an horizontal stabilizer, the pitching axis is located far upstream from the mean aerodynamic center. In this case, geometric approximations provide a relationship between pitching effect and angle of attack effect.

The pitching angular velocity creates a local velocity (Fig 7) given by

$$-\vec{q} \wedge \overrightarrow{OM} \quad .$$

In the plan (Oxy), this induced velocity field becomes

$$\overrightarrow{v_M} = (x_M - x_O).q\,\vec{k} \quad . \tag{6}$$

And so the total velocity is

$$\vec{V}_M = V_\infty\,\vec{i} + (x_M - x_O).q\,\vec{k} \quad . \tag{7}$$

Thus, the local angle of attack is :

$$\alpha_M = \tan^{-1}\left(\frac{(x_M - x_O).q}{V_\infty}\right) \quad .$$

Along the wing, this angle of attack varies (Fig. 8) between :

$$\alpha_{BA} = \tan^{-1}\left(\frac{(x_{BA} - x_O).q}{V_\infty}\right) \quad , \tag{8}$$

and

$$\alpha_{BF} = \tan^{-1}\left(\frac{(x_{BF} - x_O).q}{V_\infty}\right) = \tan^{-1}\left(\frac{(x_{BA} + C - x_O).q}{V_\infty}\right) \quad . \tag{9}$$

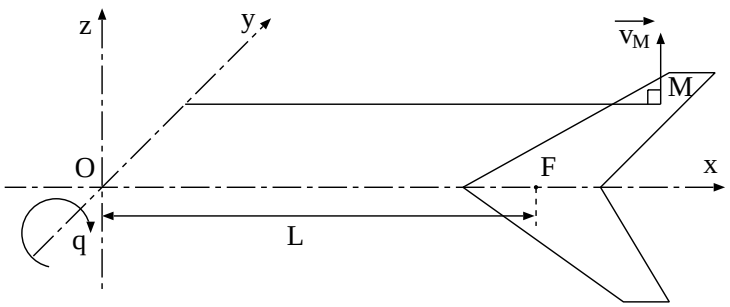

Figure 7: Local velocity induced by the rotation

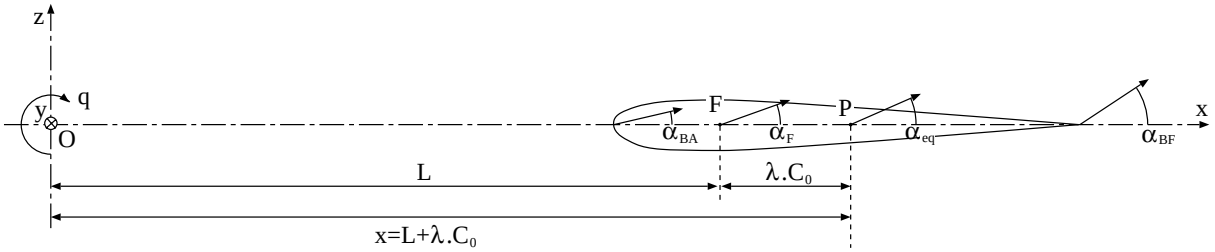

Figure 8: Locale angle of attack

When the mean aerodynamic chord is negligible compared to the lever arm ($C << (x_{BA} - x_0)$), α_{BA} and α_{BF} are almost identical and so we can assume that the local angle of attack along the span is constant.

In this case, the pitching effect becomes very similar to an angle of attack effect, and the angle of attack α_{eq} equivalent to the rotation q is bounded by α_{BA} (eqn. 8) and α_{BF} (eqn. 9). In first approximation, we can assume that α_{eq} is the local angle of attack of the mean aerodynamic center F :

$$\alpha_{eq} = tan^{-1}\left(\frac{L.q}{V_\infty}\right) \quad . \tag{10}$$

We can deduce successively

$$\tan\alpha = \frac{L.q}{V_\infty} \quad , \tag{11}$$

$$(1 + \tan^2 \alpha)\partial\alpha = \frac{L}{V_\infty}\partial q \quad , \tag{12}$$

$$\frac{\partial\alpha}{\partial q} = \frac{L/V_\infty}{1 + (L.q/V_\infty)^2} \quad , \tag{13}$$

$$\left(\frac{\partial C_z}{\partial q}\right) \Big/ \left(\frac{\partial C_z}{\partial \alpha}\right) = \frac{L/V_\infty}{1 + (L.q/V_\infty)^2} \quad , \tag{14}$$

and

$$\frac{C_{z_q}}{C_{z_\alpha}} = \left(\frac{\partial C_z}{\partial(\frac{C_0.q}{V_\infty})}\right) \Big/ \left(\frac{\partial C_z}{\partial \alpha}\right) = \frac{L/C_0}{1 + (L.q/V_\infty)^2} \quad . \tag{15}$$

For small angle of attack, $(L.q/V_\infty)^2 << 1$, so we can rewrite the final relationship :

$$\frac{C_{z_q}}{C_{z_\alpha}} = \frac{L}{C_0} \tag{16}$$

According to simulation results (cf next section), this approach did not give an accurate prediction C_{z_q}. Because the point of equivalent angle of attack is not necessarily located in F, we added a correcting term $(\lambda.C_0)$ to take into account the distance between the point F and the point of equivalent angle of attack P (Fig. 8). In this case, the final equation is changed into :

$$\frac{C_{z_q}}{C_{z_\alpha}} = \frac{L}{C_0} + \lambda \tag{17}$$

The difficulty comes from the determination of λ. This parameter can vary with geometry characteristics and with flow conditions. The use of numerical simulations allows to solve this problem.

In this approach, two assumptions were made : $\frac{L}{C_0} >> 1$ and $(L.q/V_\infty)^2 << 1$, the first one corresponds to horizontal stabilizers, the second one is always satisfied in the dynamic derivative approach : small variations of flight conditions around equilibrium.

6.3.2 Numerical validation

Parametric study The first test consists in calculating the pitch damping coefficient for many lever arms and with two different Mach numbers. The objectives are to validate the geometric approach and to determine the parameter λ (eqn. 17).

$Mach$	$\frac{L}{C_0}$	$\frac{C_{z_q}}{C_{z_\alpha}}$	$\frac{C_{z_q}}{C_{z_\alpha}} - \frac{L}{C_0}$
0.5	6	6.50	0.50
0.5	10	10.52	0.52
0.5	20	20.59	0.59
0.7	6	6.47	0.47

Table 5: Results with different lever arm

As shown in Tab.5, the expression $\frac{C_{z_q}}{C_{z_\alpha}} - \frac{L}{C_0}$ is almost independent of $\frac{L}{C_0}$ and of Mach number. So, the relationship 17 is verified and the parameter λ is equal to 0.5 : the point P is located about 0.5 chord length behind F.

Global efforts In the second test we tried to confirm the similarities between the two kinds of motion. We compared a pitching effect with two angle of attack effects.

We simulated the three following cases :

- $\alpha = 0\ deg$, $\frac{q.C_0}{V_\infty} = 0.0029$, $L = 6.735\ C_0$
- $\alpha_1 = 1.12\ deg$, $q = 0$
- $\alpha_2 = 1.19\ deg$, $q = 0$

When $\frac{q.C_0}{V_\infty} = 0.0029$ and $L = 6.735\ C_0$, the local angle of attack in F is :

$$\alpha_F = tan^{-1}\left(\frac{L.q}{V_\infty}\right) = 1.12 = \alpha_1$$

and the local angle of attack of the point located 0.5 chord length behind F is :

$$\alpha = tan^{-1}\left(\frac{(L + 0.5\ C_0).q}{V_\infty}\right) = 1.19 = \alpha_2$$

The results of the three simulations confirm the conclusions of the previous test. The efforts calculated for the q-effect are very close to the efforts calculated with the angle of attack α_2 :

$$\begin{aligned} C_z(q) &= 0.0937 & \qquad C_m(q) &= -0.633 \\ C_z(\alpha_1) &= 0.0879 & \qquad C_m(\alpha_1) &= -0.592 \\ C_z(\alpha_2) &= 0.0935 & \qquad C_m(\alpha_2) &= -0.630 \end{aligned}$$

Moreover, this comparison shows that the equivalence between the two effects is also valid for the pitching moment, and thus, for the aerodynamic center.

Conclusion This longitudinal validation shows the great interest in using numerical simulations in flight stability study. A simple geometric approach can not provide an accurate empirical relation to predict dynamic derivatives, and numerical simulations can be useful to perform parametric studies that are necessary to improve those methods. Moreover, they provide much local information, which is very interesting to better understand complex phenomena.

7 COMPLEX AIRCRAFT GEOMETRY

In this paragraph, we try to assess the ability of the numerical tool to correctly predict the steady dynamic derivatives on a complex aircraft geometry. The calculated geometry is a transport civil aircraft on which the DLR has performed some wind tunnel tests in NWB (Braunchweig). It is composed of the fuselage, the wing with its winglets, and the horizontal and vertical tailplanes. We only investigated the longitudinal derivatives at subsonic velocity. A multiblock structured mesh has been generated for this geometry. It is composed of 48 blocks and 3 millions nodes. Figure 9 shows the symmetry plane ($y = 0$) of this mesh.

On this configuration, we first performed a Navier-Stokes calculation with no rotating velocity ($q = 0$). The calculation parameters are :

- Mach number = 0.207,
- Angle of attack = 3°,
- Reynolds number = $4.74\ .\ 10^6$,
- Turbulence model of Spalart-Allmaras

The numerical results were compared with wind tunnel measurements. The relative error is less than 4% for C_{z_α} and about 10% for C_{m_α}. This agreement between the results ensure the reliability of this reference calculation.

In order to estimate the longitudinal derivatives with respect to the pitching velocity, a calculation with a non-zero value of q is performed. The coefficients are then computed by finite differences between the two computational results : $\dfrac{C_i(q) - C_i(q=0)}{q}$ (cf eqn. 4).

The unsteady contributions $C_{z_{\dot\alpha}}$ and $C_{m_{\dot\alpha}}$ have been retrieved from the experimental results for which these coefficients cannot be obtained separately from the steady ones (C_{z_q} and C_{m_q}). These unsteady coefficients have been estimated by an engineering method.

The comparison shows fair agreement between numerical and experimental results : the relative error is about 9% for C_{z_q} and 13% for C_{m_q}. For these coefficients, the level

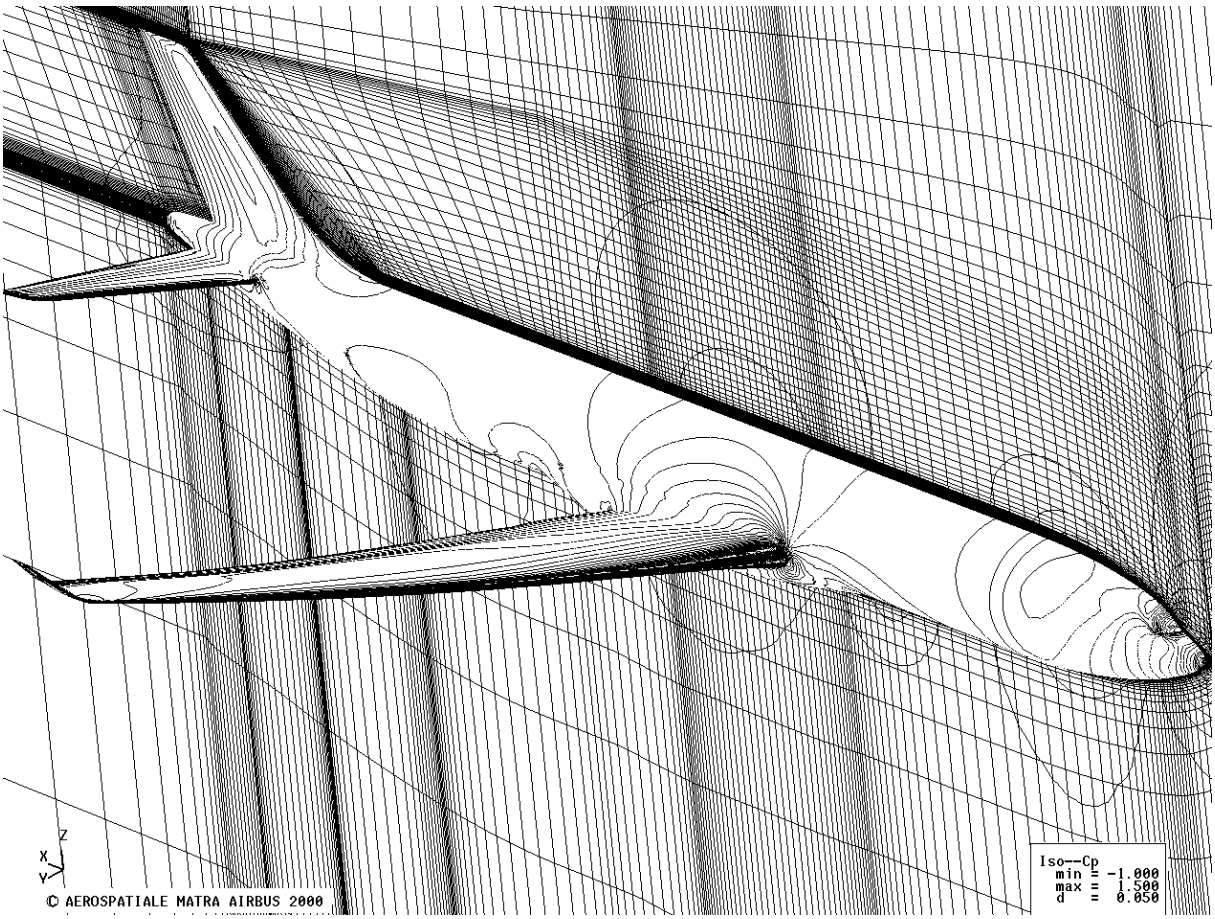

Figure 9: Mesh and pressure coefficient isolines for q-effect

of disparity between numerical and experimental results is compatible with the accuracy requirement from aircraft manufacturers regarding handling qualities. Furthermore, CFD gives access to local information (Fig. 9), which can be of great help for the understanding of the complex flow phenomena involved in this kind of motion.

8 CONCLUSION

A numerical method for the calculation of dynamic derivatives has been described. This method consists in using the ALE (Arbitrary Lagrangian Euler) formulation for the motion modelization. The ALE method used was slightly simplified with respect to Donea's formulation : the meshes are moving without any deformation.

Validation has been performed by applying the numerical method to tri-dimensional

test cases based on the ONERA M6 wing geometry. For these simple test cases, we compared the numerical results with validated engineering methods. The comparison demonstrated the capability of the numerical tool to accurately predict steady dynamic derivatives on simple geometries.

Derivatives for a complex transport civil aircraft geometry were then calculated. The calculated configuration consists of a fuselage, a wing and the horizontal and vertical tailplanes. The results were compared with experimental data from DLR. Good agreement was shown, allowing us to be optimistic for the use of this numerical tool on complex geometries.

This preliminary study demonstrates the promising perspectives related to the use of this numerical tool for the industrial prediction of the steady dynamic derivatives of complex civil aircraft geometries. Some complementary studies are needed :

- The validation of complex geometries will be continued.
- Investigations of extreme aerodynamic conditions (high Mach number, high angle of attack) will be made.
- Unsteady simulations will be performed in order to assess the numerical ability to predict derivatives with respect to variation of angle velocities.

References

[1] J.B. Vos, A.W. Rizzi, A. Corjon, A. Chaput & E. Soinne, "Recent Advances in Aerodynamics inside the NSMB (Navier-Stokes Multiblock) Consortium", *AIAA Paper 98-0225*, 1998.

[2] A. Jameson, W. Schmidt & E. Turkel, "Numerical Solutions of the Euler Equations by Finite Volume Methods Using Runge-Kutta Time Stepping", *AIAA paper 81-1259*, 1981.

[3] S. Yoon, A. Jameson, "A Multigrid LU-SSOR Scheme for Approximate Newton Iteration Applied to the Euler Equations", *NASA-CR-179524*, 1986.

[4] B. S. Baldwin and H. Lomax, "Thin Layer Approximation and Algebraic Model for Separated Turbulent Flows", *AIAA-paper 78-257*, 1978.

[5] P.R. Spalart and S.R. Allmaras, "A One-equation Turbulence Model for Aerodynamic Flows", *AIAA-paper 92-0439*, Jan. 1992.

[6] J. Donea, S. Giuliani, J. P. Halleux, "An Arbitrary Lagrangian-Euler Finite Element Method For Transient Dynamic Fluid-Structure Interactions", *Comp. Meth. in Applied Mechanics and Engineering, 33, pp689-723*, 1982.

[7] S. Champagneux, "Vers le couplage fluide-structure - Méthode ALE pour l'aerodynamique instationnaire", *Rapport de DEA, INPT, Toulouse, France*, Sept. 1997.

[8] V. Schmitt and F. Charpin, "Pressure distribution on the ONERA-M6-Wing at transonic Mach number", *AGARD AR-138, Experimental Data Base for computer program assessment, B1.1-B1.44*, May 1979.

[9] B. Etkin and L. D. Reid, "Dynamic of flight - Stability and control (Third edition)", *Ed. John Wiley & Sons*, 1996.

[10] J. Roskam "Airplane flight dynamics and automatic flight controls", *University of Kansas, Lawrence, Kansas*, 1979.

[11] ESDU, "Aerodynamics, Stability of Aircraft", *Vol. 9a, 9b, 9c, 9d, 9e*, http://esdubeta.ihs.com/.